UC Irvine
UC Irvine Previously Published Works

Title
Cofilin Activation Is Temporally Associated with the Cessation of Growth in the Developing Hippocampus.

Permalink
https://escholarship.org/uc/item/0jb3x181

Journal
Cerebral Cortex, 27(4)

ISSN
1047-3211

Authors
Lauterborn, Julie C
Kramár, Enikö A
Rice, Jeffrey D
et al.

Publication Date
2017-04-01

DOI
10.1093/cercor/bhw088

Peer reviewed

eScholarship.org Powered by the California Digital Library
University of California

Cerebral Cortex, 2016, 1–12

doi: 10.1093/cercor/bhw088
Original Article

ORIGINAL ARTICLE

Cofilin Activation Is Temporally Associated with the Cessation of Growth in the Developing Hippocampus

Julie C. Lauterborn[1], Enikö A. Kramár[1], Jeffrey D. Rice[1], Alex H. Babayan[1], Conor D. Cox[1], Carley A. Karsten[1], Christine M. Gall[1,2] and Gary Lynch[1,3]

[1]Department of Anatomy and Neurobiology, [2]Department of Neurobiology and Behavior and [3]Department of Psychiatry and Human Behavior, University of California at Irvine, Irvine, CA 92697, USA

Address correspondence to Christine Gall, Department of Anatomy and Neurobiology, 3123 Gillespie Neuroscience Research Facility, University of California, Irvine, CA 92697-1275, USA. Email: cmgall@uci.edu; cmariegall@gmail.com

Downloaded from http://cercor.oxfordjournals.org/ at University of California, Irvine on April 13, 2016

Abstract

Dendritic extension and synaptogenesis proceed at high rates in rat hippocampus during early postnatal life but markedly slow during the third week of development. The reasons for the latter, fundamental event are poorly understood. Here, we report that levels of phosphorylated (inactive) cofilin, an actin depolymerizing factor, decrease by 90% from postnatal days (pnds) 10 to 21. During the same period, levels of total and phosphorylated Arp2, which nucleates actin branches, increase. A search for elements that could explain the switch from inactive to active cofilin identified reductions in β1 integrin, TrkB, and LIM domain kinase 2b, upstream proteins that promote cofilin phosphorylation. Moreover, levels of slingshot 3, which dephosphorylates cofilin, increase during the period in which growth slows. Consistent with the cofilin results, in situ phalloidin labeling of F-actin demonstrated that spines and dendrites contained high levels of dynamic actin filaments during Week 2, but these fell dramatically by pnd 21. The results suggest that the change from inactive to constitutively active cofilin leads to a loss of dynamic actin filaments needed for process extension and thus the termination of spine formation and synaptogenesis. The relevance of these events to the emergence of memory-related synaptic plasticity is described.

Key words: actin, Arp2, Lim kinase, long-term potentiation, slingshot

Introduction

Dendritic growth and synapse formation in rat hippocampus proceed at a very high rate for the first 3 postnatal weeks, but then slow dramatically over the next several days until stable adult values are reached (Cowan et al. 1980; Gall and Lynch 1980; O'Kusky et al. 2000). Why growth stops is one of the more fundamental questions in biology, particularly given that it is not inevitable; there are vertebrate species in which body length steadily increases throughout life (Patnaik 1994; Laver et al. 2012). But applied to mammalian brain, the question has received surprisingly little attention despite its fundamental significance and broad relevance. There are, however, reasons to suspect that the termination event involves major changes in the regulation of the spine and subsynaptic cytoskeletons. Signaling cascades that control the assembly and disassembly of actin filaments exert potent influences on the formation and elaboration of dendrites during development (Lafont et al. 1993; Jan and Jan 2010; Arikkath 2012; Lanoue et al. 2013). The activity or concentrations of many elements in these actin management systems clearly differ in the neonatal versus adult brain (Dudek and Johnson 1995; Komagome et al. 2000; Zhong et al. 2003), but when these changes occur and, in particular, if they align with the cessation of growth have not been studied.

Accordingly, we used biochemical methods to test for marked shifts in the activity or concentrations of proteins that control the formation or stabilization of actin filaments from postnatal days (pnds) 10 to 42. A number of elements were assayed to address the critical question of whether any such effects involve a

© The Author 2016. Published by Oxford University Press. All rights reserved. For Permissions, please e-mail: journals.permissions@oup.com

system-wide adjustment or are discrete in nature. Results indicate that the actin depolymerizing factor cofilin (Bamburg 1999; Mizuno 2013) undergoes a marked shift into its active (dephosphorylated) state during the period in which dendritic growth and synaptogenesis abruptly slow. We then identified upstream changes that may be cause for the cofilin effect and examined a strong prediction that follows from it: That concentrations of dynamic actin filaments in spines and dendrites will decrease markedly during the third postnatal week. Together, the results point to an explicit hypothesis for the mechanisms underlying the cessation of growth and reduction in structural plasticity in hippocampus.

Materials and Methods

Experiments were conducted in accordance with the National Institutes of Health "Guide for the Care and Use of Laboratory Animals" and with procedures approved by the University of California at Irvine Animal Care and Use Committee. Sprague–Dawley male rats from 10 to 42 days of age were used with pups of multiple ages obtained from each litter for the majority of the studies; sex of younger animals was determined by anogential distance. Exact ages and group sizes are given in the Results section for each experiment.

Western Blot Analysis

Western blotting was conducted as described previously (Rex et al. 2009). Hippocampal tissue was homogenized in RIPA buffer (50 mM Tris–HCl, pH 7.4, containing 1% IGEPAL CA-630, 0.25% Na-deoxycholate, 150 mM NaCl, and 1 mM EDTA, with 1× Roche Protease Inhibitor Cocktail, 1 mM Na_3VO_4, and 1 mM NaF). Samples (30 ng of total protein in Laemmli buffer) were run for 10–12% PAGE. Blots were blocked for 1 h at room temperature (RT) with 5% milk, 1% BSA in Tris-buffered saline with Tween 20 (TBS-T), and incubated in primary antisera overnight in 5% milk or BSA in TBS-T at 4 °C. Blot studies used mouse antisera to actin (1 : 200 000, #A5441, Sigma-Aldrich), cofilin (1 : 8000, #AB54532, Abcam), slingshot 3 (SSH3; 1 : 250, #sc-390058, Santa Cruz Biotechnology), and tubulin (1 : 200 000, #T4026, Sigma-Aldrich), and rabbit antisera to the adenosine A1 receptor (A1R; 1 : 2000, #A-268, Sigma-Aldrich), actin-related protein 2 (Arp2; 1 : 750, #SC-15389, Santa Cruz Biotechnology), phosphorylated (p) Arp 2 Thr237/238 (1 : 1000, #AP3871, ECM Biosciences), brain-derived neurotrophic factor (BDNF; 1 : 2000, #R-088-100, Novus Biologicals), pCofilin Ser3 (1 : 8000, #Ab12866, Abcam), cortactin (1 : 6000, #sc-11408, Santa Cruz Biotechnology), pCortactin Y466 (1 : 2000, #Ab51073, Abcam), integrin β1 (1 : 1000, #MAB1997, EMD Millipore), LIM Kinase 1 (LIMK1; 1 : 1000, #3842, Cell Signaling Technology), LIMK2 (1 : 500, #sc-5577, Santa Cruz Biotechnology), pyridoxine 5′-phosphate phosphatase (PDXP; 1 : 6000, #4686, Cell Signaling Technology), slingshot 1 (SSH1; 1 : 375, #SP1711, ECM Biosciences), testis-specific protein kinase 1 (TESK1; 1 : 500, #ab92707, Abcam), TESK2 (1 : 1500, #LS-C200773, LS Biosciences), TrkB (1 : 2000, #07-225, EMD Millipore), and pTrkB Tyr817 (1 : 2000, #gtx61736, Genetex). Horseradish peroxidase-conjugated anti-rabbit and anti-mouse secondary antibodies (1 : 10 000, Amersham) were incubated for 1 h in 5% milk in TBS-T at RT. Blots were processed for chemiluminescence (Amersham ECL Prime, GE) and analyzed with ImageJ or Image Studio (LiCor) for densitometric measures. Values were normalized to sample tubulin content. Significance was determined by 1-way ANOVA, followed by post hoc analyses using Tukey's or Newman–Keuls multiple comparison tests.

Co-immunoprecipitation

Rats at pnds 10 and 21 were killed by decapitation, and the hippocampus was rapidly dissected free over ice, fresh-frozen, and stored at −80 °C until analysis. Tissue was homogenized in RIPA buffer and processed for co-immunoprecipitation using goat anti-cofilin (1 µL/190 µg protein; #sc-8441, Santa Cruz Biotechnology) and protein A/G plus-agarose (sc-2003, Santa Cruz Biotechnology) according to vendor instructions. Samples were separated using 8–12% PAGE, and blots were processed as above using goat anti-cofilin (1 : 200, #sc-8441), mouse anti-SSH3 (1 : 50, #sc-390058), or rabbit anti-TESK1 (1 : 100, #ab92707). For each sample, levels of SSH3 or TESK1 labeling were expressed as a ratio to cofilin labeling. Significance of group differences for each protein was determined using a Student's *t*-test.

Immunocytochemistry for pCofilin

Rats were anesthetized with an overdose of euthasol and intracardially perfused with 4% paraformaldehyde in 0.1 M phosphate buffer (PB, pH 7.4). Brains were post-fixed in perfusate for 2 h, cryoprotected in 20% sucrose/0.1 M PB, and sectioned at 30 µm on the coronal plane using a freezing microtome. Tissue sections from each developmental age ($n = 6$ per age) were slide-mounted and processed together for either brightfield immunohistochemistry or dual immunofluorescence microscopy.

For the light microscopic evaluation of regional pCofilin immunolabeling in hippocampus, tissue was incubated in rabbit anti-pCofilin Ser3 (1 : 800; #Ab12866, Abcam) for 24 h at 4 °C and then processed using the VECTASTAIN Elite ABC method with biotinylated anti-rabbit IgG (Vector Labs) and 3,3′-diaminobenzidine as chromagen. Brightfield photomicrographs were acquired on an Olympus AX70 microscope using a ×10 objective.

Studies of the synaptic localization of pCofilin used dual immunofluorescence as described previously (Chen et al. 2007; Seese et al. 2012) and a primary antisera cocktail including rabbit anti-pCofilin Ser3 (1 : 800, #Ab12866, Abcam) and mouse anti-PSD95 (1 : 1000, #MA1-045, Thermo Scientific) for 24 h at 4 °C and AlexaFluor secondary antibodies (594 goat anti-rabbit IgG and 488 goat anti-mouse IgG; both at 1 : 1000). Image z-stacks were collected from hippocampal field CA1 stratum radiatum from 5 to 7 sections per brain: Images were captured at 0.2 µm steps through a depth of 2 µm using a Leica DM6000B epifluorescence microscope with a ×63 objective for a sample field size of 105 × 136 × 2 µm (28 560 μm^3 per sample field). The images were processed for fluorescence deconvolution tomography (Seese et al. 2013) to quantify immunolabeling of synaptic elements. Thus, individual z-step images were processed through iterative deconvolution (Volocity 4.1; Perkin Elmer), and then in-house software was used to construct 3-dimensional (3D) montages and quantify double-labeled (e.g., both pCofilin- and PSD95-immunoreactive) or single-labeled puncta within the size constraints of synapses as in prior work (Rex et al. 2009; Chen et al. 2010; Seese et al. 2013). Briefly, individual images were normalized to 30% of maximum background intensity and iteratively binarized at regular intensity thresholds using exclusion criteria for object size and ellipticity optimized for spine detection, followed by dilation and erosion filtering. Repeated observations were binned and analyzed to identify object boundaries and to discriminate neighboring objects. Objects were then reconstructed in 3D to calculate volume and position. For each image stack, the areas of labeling with each fluorophore were evaluated independently, and objects were considered double-labeled if boundaries occupied by the different fluorophores overlapped

Downloaded from http://cercor.oxfordjournals.org/ at University of California, Irvine on April 13, 2016

as viewed in 3D. Counts of single- and double-labeled puncta were averaged to produce individual animal means that were then averaged to generate group mean ± SEM values. Significant differences between 2 groups were determined using a Student's t-test.

Electrophysiology and In Situ Phalloidin Labeling

Acute hippocampal slices were prepared from male rats (pnds 11, 12, 16, 21, and 42) at a thickness of 350 µm and maintained in an interface recording chamber as described previously (Kramar and Lynch 2003; Rex et al. 2009; Trieu et al. 2015). The chamber was continually perfused (1–1.5 mL/min) with preheated artificial cerebrospinal fluid (ACSF) containing (in mM) 124 NaCl, 3 KCl, 1.25 KH_2PO_4, 1.5 $MgSO_4$, 2.5 $CaCl_2$, 26 $NaHCO_3$, and 10 glucose, and maintained at 31 ± 1 °C. The surface of the slices was exposed to warm, humidified 95% O_2/5% CO_2. Recordings began 2 h after incubation.

Field excitatory synaptic potentials (fEPSPs) were recorded from CA1b stratum radiatum using a single glass pipette filled with 2 M NaCl (2–3 MΩ) in response to orthodromic stimulation of Schaffer–commissural (S–C) projections in CA1c stratum radiatum (Trieu et al. 2015). Current intensity was adjusted to obtain 50–60% of the maximum spike-free fEPSP. Following a 20-min stable baseline, latrunculin A was introduced into the infusion line for a final bath concentration of 200 nM (Rex et al. 2010). Data were collected and digitized by the NAC 2.0 Neurodata Acquisition System (Theta Burst Corp.) and stored on a disk.

The in situ phalloidin-labeling method was performed as described previously (Gohla et al. 2005; Kramar et al. 2006, 2009; Rex et al. 2007). Following a 2-h post-preparation incubation period, slices were randomly divided into 3 groups: 1) "control" that received low-frequency stimulation of S–C projections at 0.05 Hz for 30 min, 2) "drug treated" that were incubated with 200 nM latrunculin A for 30 min, or 3) "theta frequency activity" which entailed stimulation of the S–C projections with 10 theta bursts of 4 pulses at 100 Hz with an interburst interval of 200 ms. At the end of the experiment, each slice received 4 topical applications of Alexa Fluor-568 phalloidin (6 µM in ACSF; Trocis) with 5 min between each application. Slices were then fixed in 4% paraformaldehyde and prepared for microscopy. Labeling was examined using a Carl Zeiss Axioskop microscope (×40) and an Axiocam camera. Identification and quantification of labeled spines were as described (Lin et al. 2005; Kramar et al. 2006). For each field, 5 sequential images were collected at 2 µm focal steps totaling a thickness of 10 µm on each z-axis. Significance was determined either by 1-way ANOVA for effects of age or by 2-way ANOVA for the comparison of effects of age and latrunculin A.

Post-Fixation Phalloidin Labeling

Fresh-frozen brains were cryostat-sectioned (20 µm, coronal), and slide-mounted sections were fixed with 4% paraformaldehyde. Sections through the hippocampus were incubated with rhodamine phalloidin (1 : 500; Cell Signaling Technology) in 0.1 M PB containing 3% BSA and 0.3% Triton-X for 1 h at RT and examined using an epifluorescence microscope (Leica DM6000) with a ×40 PlanApo objective and a CCD camera (ORCA-ER, Hamamatsu). Single-plane images were collected from CA1 stratum radiatum. For each image, a 40-pixel Gaussian blur was subtracted to normalize fluorescence intensity background. Then, the mean gray value for the entire field of each image was calculated using the FIJI Measure tool (NIH). Mean intensity measures per animal were obtained from 5 images, and group means were calculated. Significance was determined by 1-way ANOVA, followed by post hoc analyses using Tukey's multiple comparison test.

Results

Cofilin Switches to an Active (Dephosphorylated) State by the End of Week 3

Western blots were used to estimate protein concentrations in the hippocampus from pnd 10 to young adulthood. Total hippocampal levels of actin and tubulin were fairly constant over this period (ANOVA: actin, $P = 0.6283$, tubulin, $P = 0.1811$; Fig. 1A,B), indicating that sample preparation and immunolabeling were not systematically affected by developmental changes in the size and composition of the hippocampus.

We began analyses of actin regulatory agents with cofilin, a constitutively active protein that severs actin filaments (Bamburg 1999; Mizuno 2013). Phosphorylation of cofilin at serine 3 causes inactivation (Moriyama et al. 1996), thereby allowing survival of elongating filaments. Total cofilin concentration was relatively constant from pnd 10 to 42 ($P = 0.3243$, ANOVA). In striking contrast, hippocampal levels of phosphorylated (p) cofilin decreased dramatically from pnd 10 to 16 ($P < 0.0001$, ANOVA; $P < 0.05$ for pnd 10 vs. 16, Tukey's), with still lower levels reached by pnd 21 (Fig. 1A,C). The ratio of phosphorylated to total cofilin levels was reduced nearly 90% from pnd 10 to 21 ($P = 0.0005$, ANOVA; $P < 0.001$ for pnd 10 vs. 21, Tukey's). These results provide the first evidence that cofilin switches from its inactive to its active state during hippocampal development in synchrony with the decline in dendritic growth and synaptogenesis (O'Kusky et al. 2000).

Next, we asked whether the extremely sharp decline in levels of pCofilin during Week 3 is typical of actin management proteins. Cortactin, a monomeric protein that facilitates the organization of newly formed filaments into actin networks (Ammer and Weed 2008), decreased by ~30% during Week 3, but this held for both total and phosphorylated (activated) forms (for both: $P < 0.002$, ANOVA; $P < 0.01$ for pnd 10 vs. 21, Tukey's; Fig. 1D). Activated cortactin recruits Arp2/3 complex proteins to actin filaments, thereby creating nucleation sites for actin branch formation and the stabilization of filaments. Levels of total and phosphorylated (activated) Arp2 increased 2.7- and 1.9-fold, respectively, from pnd 10 to 21, and then rose somewhat further by pnd 42 (for both: $P < 0.0001$, ANOVA; pnd 10 vs. 21, $P < 0.001$, Tukey's; Fig. 1A,D). It thus appears, from this limited sample, that the pattern of change in levels of pCofilin is not typical of other actin-associated proteins.

We investigated possible reasons that cofilin abruptly shifts to an activated state during Week 3, beginning with 3 synaptic receptors shown in previous work to regulate phosphorylation of the protein (Rex et al. 2007, 2009; Kramar et al. 2009): TrkB, the A1R, and β1 family integrins. BDNF acting through its synaptic TrkB receptor drives increases in levels of pCofilin in the hippocampus (Rex et al. 2007). Levels of TrkB phosphorylated at the tyrosine 817 autoactivation residue fell by 50% during the third postnatal week ($P = 0.0058$, ANOVA; $P < 0.05$ for pnd 14 vs. 21, Newman–Keuls) (Fig. 2A), whereas total hippocampal TrkB levels were not changed over this same period (Fig. 2A). Since TrkB drives cofilin phosphorylation, the observed reduction in activated pTrkB could be a major contributor to cofilin dephosphorylation. The decrease in pTrkB was seemingly not due to a developmental decline in BDNF ligand, because hippocampal levels of mature, 14 kDa BDNF increased steadily from pnd 10 to pnd 42 ($P < 0.0001$, ANOVA; Fig. 2A).

Downloaded from http://cercor.oxfordjournals.org/ at University of California, Irvine on April 13, 2016

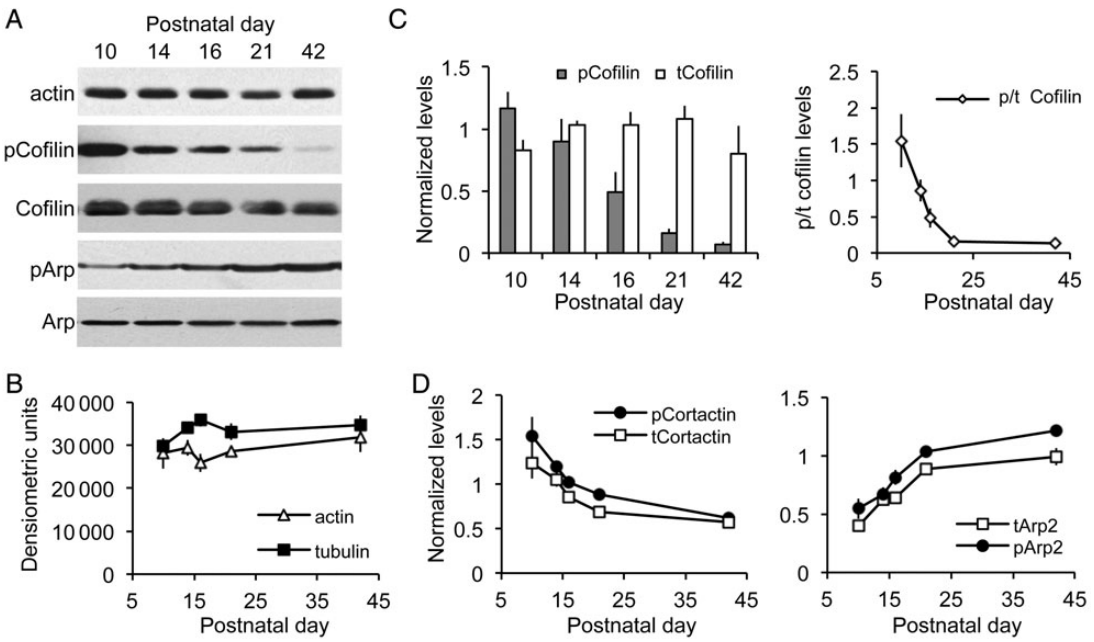

Figure 1. Hippocampal cofilin shifts from an inactive to an active state during the third postnatal week. (*A*) Representative western blots of whole hippocampal homogenates show relative levels of actin, phosphorylated (p) and total (t) Cofilin, pArp2 and tArp2 proteins at postnatal days 10 through 42. (*B*) Densitometric measures of western blots show that actin and tubulin levels are relatively stable across ages. (*C*) Measures of western blot cofilin levels (as in *A*). *Left*, Plot shows that tCofilin protein content did not vary much over ages, whereas there was a marked drop in pCofilin content beginning at pnd 16. *Right*, Plot shows the decline in the ratio of pCofilin to tCofilin levels: the lowest relative pCofilin content was attained by pnd 21. (*D*) Densitometric measures from western blots of normalized levels of pCortactin and tCortactin (left) and of pArp2 and tArp2 (right) across postnatal ages. All values are group means ± SEM ($n = 4$–6 per age); measures in *C* and *D* were normalized to tubulin content from the same samples.

Synaptic adhesion receptors belonging to the β1 family of integrins (i.e., integrins containing a β1 subunit) are also known to drive synaptic cofilin phosphorylation (Wang et al. 2008). As with activated TrkB, hippocampal levels of β1 integrin declined by ~50% from pnd 10 to 21 ($P = 0.0143$, ANOVA; pnd 10 vs. 21, $P < 0.05$, Tukey's; Fig. 2*B*), thus introducing a second factor that could contribute to an abrupt decrease in cofilin phosphorylation over the same age range. Finally, we have determined that signaling from the A1Rs, which are abundant throughout the hippocampus (Rex et al. 2005), blocks cofilin phosphorylation and actin polymerization in adult hippocampus (Rex et al. 2009). A developmental increase in A1Rs would thus be expected to contribute to the shift in cofilin state during Week 3. However, levels of A1Rs decreased markedly during this period (Fig. 2*B*). In all, these experiments identified developmental decreases in 2 factors—pTrkB and β1 integrin—that initiate cofilin phosphorylation and so could account for the transfer of the protein into its active state.

Developmental Changes in Enzymes That Regulate Cofilin Phosphorylation

Next, we investigated kinases targeting cofilin as potential contributors to the developmental change in cofilin activation. LIMK1/2 and the testis-specific kinases TESK1/2 are the 2 major kinases known to directly phosphorylate cofilin (Mizuno 2013). Hippocampal levels of total LIMK1 protein did not significantly change from 10 to 42 days of age ($P = 0.5726$, ANOVA) (Fig. 3*A*). The 2 LIMK2 isoforms (2a and 2b) had different expression patterns: LIMK2a levels increased moderately through the development window ($P = 0.0512$, ANOVA), whereas LIMK2b levels slowly decreased by 86% over the same age range ($P = 0.0264$, ANOVA; $P < 0.05$, pnd 10 vs. 42, Tukey's) (Fig. 3*A*). In contrast, TESK1 levels decreased sharply from pnd 10 to 14 ($P < 0.05$, Tukey's; $P = 0.0015$, overall ANOVA) and remained fairly constant thereafter (Fig. 3*A*). TESK2 levels did not significantly change from pnd 10 to 42 ($P = 0.2836$, ANOVA). These results suggest that the downregulation of 2 cofilin-targeting kinases, LIMK2b and TESK1, during the second and third postnatal weeks could also contribute to the decline in cofilin phosphorylation.

Countering the kinases are the slingshot family phosphatases (SSH 1-3) known from many cell systems to directly target pCofilin (Niwa et al. 2002; Mizuno 2013). Tests for increases in SSH from pnd 10 to 21 proved positive: total SSH3 increased 1.9-fold from pnd 10 to pnd 21 (Fig. 3*B*) ($P = 0.0002$ ANOVA; $P < 0.001$ for pnd 10 vs. 21, Tukey's), whereas SSH1 protein levels were unchanged through pnd 16, but then rose through pnd 42 ($P = 0.0016$, ANOVA) (Fig. 3*B*). Finally, pyridoxine 5'-phosphate phosphatase (PDXP; a.k.a chronophin, CIN), a haloacid dehalogenase type phosphatase that also targets cofilin (Gohla et al. 2005), was unchanged over the ages examined ($P = 0.7458$, ANOVA) (not shown).

To address which enzyme, the kinase TESK1 or phosphatase SSH3, is more likely to be involved in the loss of pCofilin during Week 3, we used co-immunoprecipitation to determine whether either protein is more closely associated with the depolymerizing factor. Antisera to total cofilin was used to precipitate the protein, and blots of the precipitates were then probed for co-precipitating SSH3 or TESK1. As shown in Figure 3*C*, levels of SSH3 co-immunoprecipitated with cofilin at pnd 21 were nearly double those found at pnd 10 ($P = 0.0017$, Student's *t*-test), whereas levels of associated TESK1 were equivalent between ages ($P = 0.949$, Student's *t*-test), suggesting that SSH activity is likely the agent responsible for cofilin dephosphorylation.

In summary, the nearly 10-fold drop in hippocampal pCofilin levels from pnd 10 to pnd 21 is likely caused by marked increases

Downloaded from http://cercor.oxfordjournals.org/ at University of California, Irvine on April 13, 2016

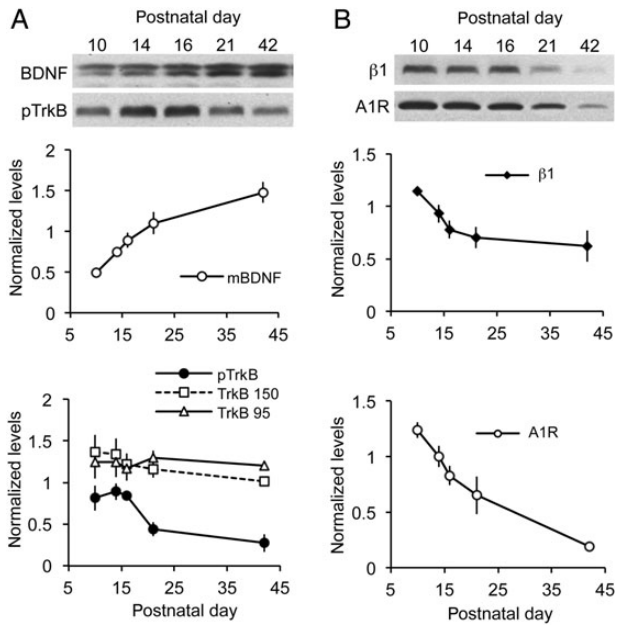

Figure 2. Developmental changes in levels of receptors and ligands that regulate cofilin phosphorylation in rat hippocampus. Western blots were used to evaluate key cofilin regulatory proteins in whole hippocampal homogenates. (*A*) *Top*, Representative blots show levels of mature (14 kDa) BDNF (mBDNF) and phosphorylated (p) TrkB Y817 across postnatal ages. *Bottom*, Normalized densitometric measures from western blots for mBDNF, pTrkB Y817, and total TrkB isoforms at 95 and 150 kDa. As shown, BDNF levels increased throughout the postnatal period, whereas pTrkB levels decreased from pnd 16 onward. Levels of total TrkB isoforms were relatively constant. (*B*) *Top*, representative blots show levels of integrin β1 and the adenosine A1 receptor (A1R) at pnd 10–42. *Bottom*, plots show normalized densitometric measures of β1 and A1R levels. Each decreased through pnd 21, although A1R levels continued to decline to pnd 42, whereas β1 levels are unchanged from pnd 21 to pnd 42. Values are means ± SEM of densitometric units normalized to tubulin measures for each sample ($n = 4$–5 per time point).

in SSH levels and association with cofilin by Week 3, with potentially smaller contributions from decreases in kinases LIMK2b and TESK1.

Developmental Changes in the Distribution of pCofilin in the Hippocampus

The marked drop in total pCofilin levels during postnatal development raises questions as to the localization of these changes. To address this, we evaluated the distribution of pCofilin immunoreactivity (ir) at pnd 10 and 21, when developmental differences were greatest. At pnd 10, pCofilin-ir was most prominently localized to diffuse bands of immunolabeling within the molecular layers of the hippocampus proper and the dentate gyrus (Fig. 4*A*,*B*). This widespread distribution is consistent with ongoing growth and elaboration of dendrites and afferent systems at these ages (Zimmer and Haug 1978). However, by pnd 21, the diffuse labeling in these fields was greatly reduced (Fig. 4*A*,*B*), consistent with the reduction in pCofilin levels seen in the blot analyses.

Synaptogenesis is rapid during the first postnatal week such that synaptic density reaches near adult levels by around pnd 25 (Crain et al. 1973; O'Kusky et al. 2000). Prior work has shown that in the adult, total and phosphorylated cofilin is preferentially localized to dendritic spines (Racz and Weinberg 2006; Chen et al. 2007; Rex et al. 2009). Consequently, we used fluorescence deconvolution tomography to assess the degree to which pCofilin localized to spines, identified with immunolabeling for the excitatory synapse marker PSD95 (Hunt et al. 1996; Kennedy 1997; Aoki et al. 2001) at pnd 10 and 21 (Fig. 4*C*). The assay used criteria optimized for identifying immunolabeled elements within the size and shape constraints of dendritic spines and spine synapses; diffuse labeling is not quantified with this method. In the CA1 stratum radiatum field of analysis, discrete PSD95 immunostaining is almost exclusively localized to spine synapses and increases from pnds 10 to 35 along with numbers of spines and synapses (Petralia et al. 2005). As shown in Figure 4*D*, PSD95-ir puncta were more numerous at pnd 21 than pnd 10 ($P < 0.0001$, Student's *t*-test). Phospho-cofilin was predominantly localized to synapse-sized puncta with little evidence for dendritic or axonal labeling. The total number of pCofilin-ir aggregates was greater at pnd 21 than 10 ($P < 0.0001$, Student's *t*-test). Dual immunolabeling demonstrated that the incidence of pCofilin/PSD95 colocalization also increased with age: the percentage of PSD95+ puncta associated with pCofilin was 50% at pnd 10 and 75% at pnd 21 ($P < 0.0001$, Student's *t*-test) (Fig. 4*D*). Taken together, the results indicate that there is an overall reduction in pCofilin levels by the third week postnatal with some portion of the remaining phosphoprotein being concentrated at postsynaptic sites.

Changes in Spine Concentrations of F-Actin During Maturation

The dramatic decrease in the ratio of pCofilin to total (t) Cofilin levels between 10 and 21 days of age (Fig. 1*C*) predicts that the third postnatal week will be marked by substantial changes in filamentous actin levels in the CA1 dendritic field. This was tested using in situ phalloidin labeling of F-actin. Fluorescence-tagged phalloidin, a toxin that binds with high selectivity to F-actin (Cooper 1987), was infused into living acute hippocampal slices prepared from rats of different postnatal ages. Past studies have shown that the bulk of phalloidin labeling occurs within dendritic spines (Lin et al. 2005; Kramar et al. 2006; Rex et al. 2007). The slices were then fixed and sub-sectioned, and labeling was viewed with epifluorescence microscopy. As shown in Figure 5*A*, there was a striking drop in phalloidin labeling from pnd 11 to pnd 21. To quantify the change within the synaptic compartment, numbers of densely phalloidin-labeled spine-sized elements were quantified for sample fields in CA1 stratum radiatum. The effect of age on these counts was striking (Fig. 5*A*): numbers of labeled puncta were unchanged from pnd 11 to 12 but then dropped significantly by 16, and declined further to near undetectable levels by Day 21 (1-way ANOVA, $F = 21$, $P = 0.0013$; $P < 0.05$ for pnd 11 vs. 16, $P < 0.01$ for pnd 11 vs. 21, Tukey's). This sharp decline in phalloidin labeling of F-actin was comparable with that found for pCofilin protein content (Fig. 1*C*) during the third postnatal week.

Next, we tested whether the high levels of F-actin prior to the third postnatal week reflected dynamic or stable polymers by briefly infusing latrunculin A into living hippocampal slices maintained in an interface recording chamber. The toxin, which selectively blocks the addition of actin monomers and thereby disrupts growing and recently formed (i.e., treadmilling) filaments (Yarmola et al. 2000), caused a rapid and pronounced loss of phalloidin labeling in stratum radiatum of field CA1 of pnd 11 slices (Fig. 5*B*); average counts of labeled spine-like elements were 1567 ± 209 (SEM) in control ($n = 6$) versus 652 ± 60 in latrunculin A-treated ($n = 7$) slices ($P < 0.001$, 2-tailed *t*-test). As expected, the low levels of staining found in the same region of adult slices were not detectably affected by the toxin (Fig. 5*B*).

To evaluate the possibility that the developmental effects might reflect age-dependent changes in the penetration of

Downloaded from http://cercor.oxfordjournals.org/ at University of California, Irvine on April 13, 2016

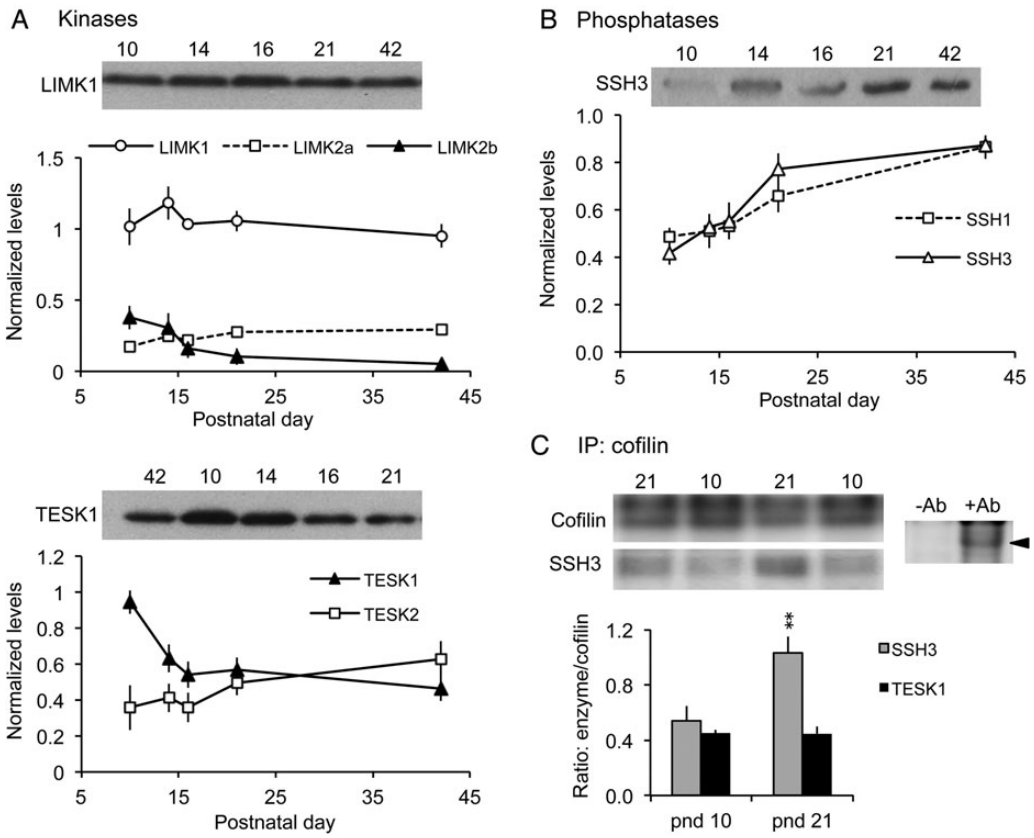

Figure 3. Levels of the cofilin phosphatase slingshot (SSH)-3 increase during the third postnatal week. (*A*,*B*) Western blots of whole hippocampal homogenates were used to evaluate relative levels of cofilin kinases and phosphatases. For each sample, band densities were normalized to those for tubulin; group mean ± SEM values are shown for $n = 4$–6 animals samples per group. (*A*) Levels of LIMK1, LIMK2a, and TESK2 showed little change from pnd 10 to 42 (representative blots for LIMK1 and TESK1 shown). In contrast, LIMK2b levels declined from pnd 10 to 16, and TESK1 levels dropped sharply from pnd 10 to 14. (*B*) Levels of phosphatases SSH1 and SSH3 increased throughout the developmental period, with greatest SSH3 levels reached by pnd 21 (representative blot for SSH3 shown). (*C*) Co-immunoprecipitation experiments. *Top Left*, western blots show levels of cofilin and SSH3 immunoreactivities in representative samples from pnd 10 and 21 hippocampus following immunoprecipitation (IP) with anti-Cofilin. *Top right*, control experiment showing that cofilin is immunoprecipitated in the presence of goat anti-cofilin (+Ab) but not without antibody (-Ab). *Bottom*, Quantification of SSH3 and TESK1 protein levels following co-IP with anti-Cofilin. As shown, the ratio of SSH3-to-Cofilin levels was significantly greater at pnd 21 than at pnd 10 (**$P = 0.0017$, Student's *t*-test); levels of TESK1 co-immunoprecipitated with cofilin were similar at pnd 10 and pnd 21 ($P = 0.949$) ($n = 3$ per group).

phalloidin in the *ex vivo* slice, binding was measured on fixed slices. Concentrations of phalloidin labeling decreased from the second to third postnatal weeks ($P = 0.0024$, ANOVA; $P < 0.05$ for weeks 2 vs. 3, Tukey's) (Fig. 5*C*), consistent with the live tissue studies.

Decreases in Dynamic F-Actin Coincide with the Emergence of Adult Synaptic Physiology

It seems reasonable to assume that the cytoskeletal changes described above not only terminate the growth period but also profoundly change the operating characteristics of synapses that depend on spine actin function (Okamoto et al. 2007; Rex et al. 2010; Seese et al. 2013). We conducted additional experiments to test this idea.

Prior studies of the S–C projections to the CA1 apical dendritic field in immature slices did not provide an analysis of input/output relationships (Kramar and Lynch 2003), so this essential point was first tested. Measuring the size of the field EPSP (fEPSP) as a function of the size of the fiber volley (a measure of the number of axons stimulated) uncovered a dramatic difference occurring between pnd 11 and 16 in which the postsynaptic response, to the same sized input, increased 2- to 3-fold (slope comparison; 1-way ANOVA, $P = 0.0017$). Much more modest changes then occurred between Days 16 and 21 (Fig. 6*A*,*B*). These results suggest that input axons are largely in place by the end of the second postnatal week and that subsequent changes involve proliferation of synapses per fiber.

Next, we tested for developmental changes in transmitter release using paired-pulse facilitation (PPF), a physiological measure that varies inversely with release probability (Pr) (Zucker and Regehr 2002; Wasling et al. 2004). In line with prior reports that PPF increases in field CA1 across the first 2 postnatal weeks (Muller et al. 1989; Wasling et al. 2004), we found percent PPF was significantly smaller at pnd 11 than at pnd 16 or 21 (Fig. 6*C*) (2-way RM ANOVA, $F = 25.34$; $P < 0.0001$ for pnd 11 vs. 16 and 21 at 40, 60, and 100 ms). Available evidence indicates that the releasable vesicle pool does not change over this age period (Wasling et al. 2004). The lower PPF in the younger animals could therefore reflect a smaller effect on vesicle mobilization during repetitive stimulation (Muller et al. 1989) or Ca^{++} saturation of release machinery on the first pulse (Wasling et al. 2004). Together, the I/O and paired-pulse data help explain why LTP induced by theta burst stimulation is substantially smaller at pnd 11 than later in the third postnatal week (Muller et al. 1989; Jackson et al. 1993; Liao and Malinow 1996). That is, the combination of less depolarization produced by a given stimulation current and only modest frequency facilitation within a burst will result in less unblocking

Downloaded from http://cercor.oxfordjournals.org/ at University of California, Irvine on April 13, 2016

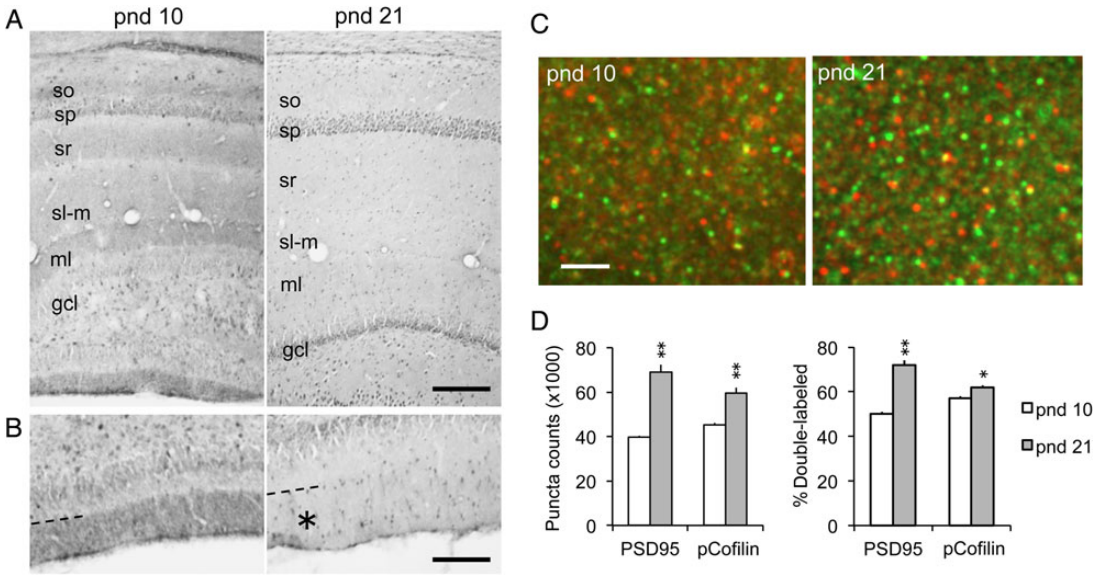

Figure 4. Hippocampal pCofilin immunoreactivity (ir) shifts from diffuse laminar to a synaptic localization with age. (*A*) Brightfield photomicrographs show pCofilin-ir in field CA1 and the dentate gyrus of pnd 10 and 21 rats. At pnd 10, there are diffuse bands of immunoreactivity in the molecular layers including strata oriens (so), radiatum (sr), and lacunosum moleculare (sl-m) in CA1, and the distal two-thirds of the molecular layer (ml) of the dentate gyrus; these fields of labeling are not evident at pnd 21 (sp, stratum pyramidale; gcl, granule cell layer; bar = 210 µm). (*B*) Higher magnification views of the external blade of the dentate gyrus at pnd 10 (left) and 21 (right) showing diffuse pCofilin-ir is confined in the distal molecular layer field of perforant path termination; this diffuse immunostaining was not present in this same field (asterisk) at pnd 21 (bar = 130 µm). (*C*) Deconvolved images show dual immunofluorescence for pCofilin-ir (red) and PSD95-ir (green), and a merge of the 2 with double-labeled elements appearing yellow, in CA1 stratum radiatum (bar, 2.5 µm). (*D*) *Left*, Quantification of PSD95-ir and pCofilin-ir puncta within size and shape constraints of synaptic elements in stratum radiatum. *Right*, Plot showing the proportion of PSD95-ir and pCofilin-ir puncta that were double-labeled at each age (group mean ± SEM values shown per 28 560 μm^3 sample field; $n = 6$ per age; $^*P < 0.01$, $^{**}P < 0.0001$ for pnd 10 vs. pnd 21, Student's *t*-test).

of voltage-dependent NMDA receptors than that occurring slightly later in development.

With these results as background, we tested the effects on synaptic responses of disrupting the high levels of dynamic actin filaments found in the immature hippocampus. Latrunculin A, infused at the same concentration that cause pronounced reductions of F-actin levels, produced a marked depression of fEPSPs recorded in the proximal, apical dendrites of field CA1b of pnd 11 slices following single pulse stimulation of the S–C projections ($P = 0.009$ for baseline vs. drug; 2-way RM ANOVA, $F = 64$). The effect had a rapid onset and did not reverse upon washout (Fig. 6*D*). Latrunculin did not detectably affect baseline physiology in adult hippocampal slices (baseline vs. drug; 2-way RM ANOVA, $F = 17.8$, $P = 0.08$). Given that latrunculin selectively influences forming and newly formed actin filaments, these results provide the first evidence that a continuous, rapid turnover of actin networks serves to maintain fast excitatory transmission in the immature, but not adult, hippocampus.

Delivery of a single train of theta burst stimulation (TBS) to the apical branch of the S–C projections elicits LTP in hippocampal field CA1 of rats as young as pnd 9–10 (Isomura and Kato 1999; Kramar and Lynch 2003). However, the remarkable stability of potentiation found in adults only emerges during the third postnatal week (Harris and Teyler 1984; Kramar and Lynch 2003). We therefore tested whether the TBS-induced increase in the number of spines containing high levels of F-actin, an effect critical for LTP stabilization (Lynch et al. 2007; Bramham 2008; Rudy 2015), occurs in slices prior to that age. TBS was administered to slices and fluorescent-tagged phalloidin was topically applied 10–15 min later; the tissue was processed for automated counting of densely phalloidin-labeled structures within the size range of dendritic spines. As shown in Figure 6*E*, TBS did not significantly influence the number of F-actin enriched spines above baseline values in pnd 11–16 hippocampal slices but caused adult-like increases at pnd 21 (1-way ANOVA, $F = 13.6$, $P = 0.0004$). It is likely that this result in part reflects the already high levels of spine F-actin in the younger slices, but it is nonetheless informative: reorganization of a relatively stable cytoskeleton by theta stimulation, an event shown in many studies to be critical for LTP consolidation, is not available until growth slows.

Discussion

Why dendritic expansion and synapse formation dramatically slow at a relatively late stage of postnatal life in mammals is one of the most fundamental, yet poorly understood, questions facing developmental neuroscience. The present studies investigated the potential origins of the rather abrupt termination of growth beginning with the assumption that they involve changes in actin management and dynamics. Process extension and retraction across cell types are driven by dynamic actin filament and acto-myosin motors, and there is considerable evidence that this also holds for spines and dendrites (Fischer et al. 1998; Hotulainen and Hoogenraad 2010; Rex et al. 2010; Koskinen et al. 2014). The effects of cofilin on actin filament assembly and disassembly are exceedingly complex and dependent upon interactions with a diverse collection of other proteins (Kedrin et al. 2007; Pak et al. 2008; Bernstein and Bamburg 2010; Courtemanche et al. 2015). A recent model (van Rheenen et al. 2009) that summarizes a great deal of material posits a cycle in which active cofilin is localized to submembrane and dynamic cytoskeletal regions (the latter termed the F-actin compartment) adjacent to a large cytosolic compartment containing phosphorylated (inactive) cofilin (van Rheenen et al. 2007; Wang et al. 2007). The protein is activated as it reaches the F-actin compartment, and there severs filaments creating free barbed ends and cofilin-G-actin complexes. The former provides sites for

Downloaded from http://cercor.oxfordjournals.org/ at University of California, Irvine on April 13, 2016

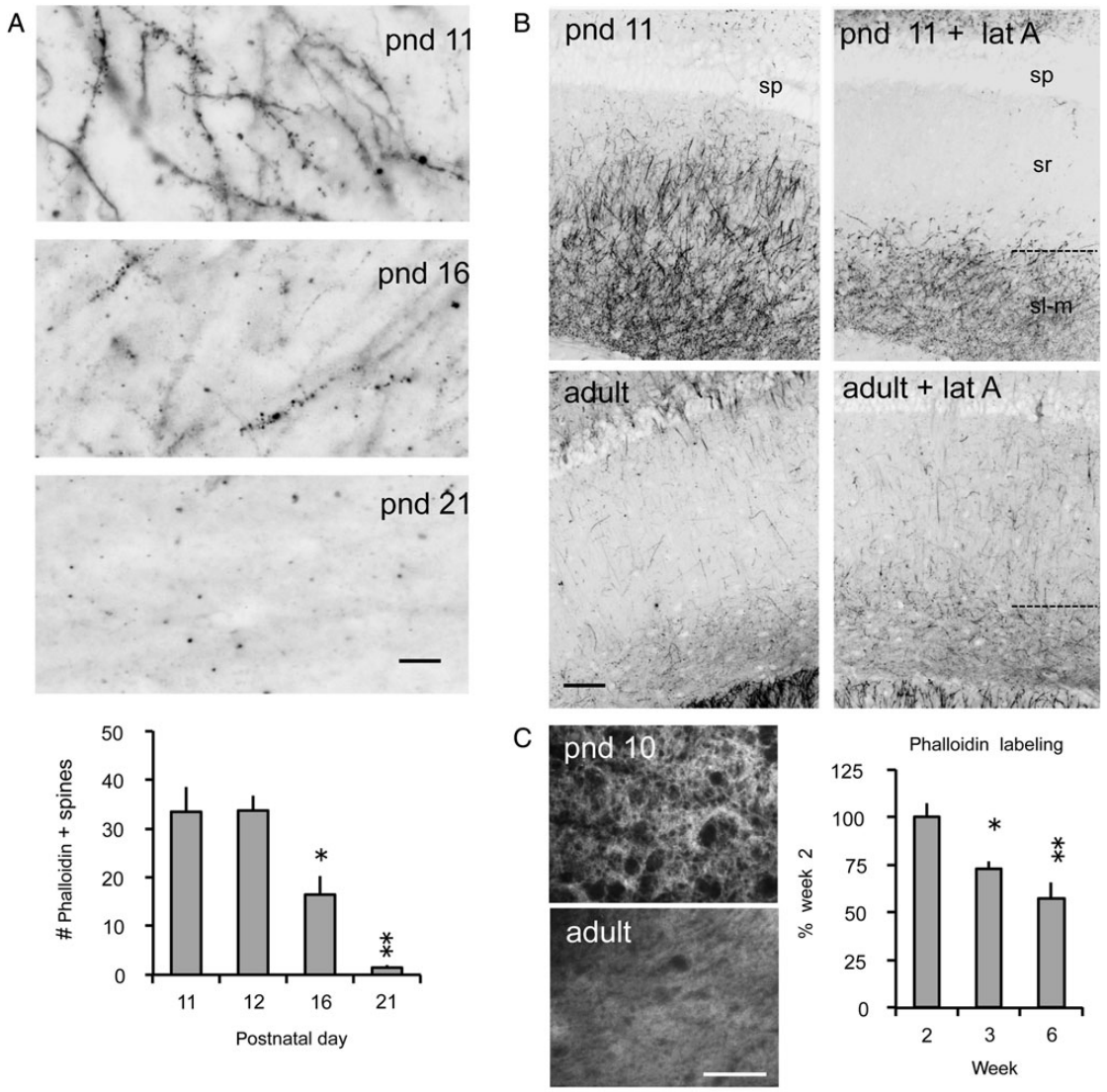

Figure 5. Dendritic and spine F-actin decreases from the second to the third postnatal week. (*A*) *Top*, Photomicrographs show that in situ phalloidin labeling of F-actin in dendrites and spines (puncta) in CA1 stratum radiatum declines markedly from pnd 11 to pnd 21 (bar, 10 µm). *Bottom*, The age-dependent reduction is also evident in counts of densely phalloidin-labeled spine-like puncta in stratum radiatum from pnd 11 to pnd 21 (mean ± SEM, per 550 μm^2; $^*P < 0.05$, $^{**}P < 0.01$ vs. pnd 11, Tukey's; $n \geq 3$ per group). (*B*) Survey photomicrographs show the distribution and density of in situ phalloidin labeling in pnd 11 and adult (pnd 42) hippocampal CA1 region of a control hippocampal slice and one treated with latrunculin A (+lat A) for 30 min. At pnd 11, the intense labeling within strata radiatum (sr) and lacunosum moleculare (sl-m) is dramatically reduced by lat A treatment. In contrast, lat A had no clear effect on the already low levels of phalloidin labeling in the adult tissue (sp, stratum pyramidale; bar = 100 µm). (*C*) Rhodamine-conjugated phalloidin was used to label F-actin in stratum radiatum of fixed hippocampal tissue from pnd 10 and adult rats. *Left*, Photomicrographs show greater phalloidin labeling in pnd 10 compared with adult tissue (bar, 40 µm). *Right*, Densitometric quantification of phalloidin labeling shows a gradual reduction over Weeks 2 (pnd 10–14), 3 (pnd 16–21), and 6 (pnd 42) plotted as a percent of Week 2 levels (mean ± SEM values shown; $^*P < 0.05$, $^{**}P < 0.01$ vs. Week 2, Tukey's; $n = 4$–7 per group).

further polymerization and protrusive force, whereas the latter complexes migrate to the cytosol (Chan et al. 2000; Sun et al. 2007). Cofilin is phosphorylated by LIMK within the cytosol resulting in the release of G-actin, and then cycles back to the plasma membrane and F-actin compartments where it is again engaged in filament severing. This pattern of localized activation and global inactivation of cofilin (Wang et al. 2007; van Rheenen et al. 2009), which ensures that process extension is directional, is consistent with the high levels of phosphorylated protein within the cytosol during active postnatal growth, as observed in the present study.

The dramatic shift in cofilin phosphorylation was associated with an equally pronounced decrease in levels of F-actin in spines and dendrites, as demonstrated by phalloidin labeling. Actin filaments in growing processes are dynamic in that they continuously add monomers at the growing tip and lose them at the other end, an arrangement that provides propulsive force for extension. Dynamic filaments are disrupted by latrunculin A (Yarmola et al. 2000), and we found that the toxin greatly reduces F-actin levels in the hippocampus during the second postnatal week. The question then arises as to why the abundant F-actin present prior to the third week of maturation is not converted into stable cytoskeletal (structural) networks. Cortactin and the Arp2/3 complex play prominent roles in the branching and stabilization of such networks across cell types. While total and activated cortactin levels decreased slightly during the critical week, total and activated Arp2 levels nearly doubled; Arp2

Downloaded from http://cercor.oxfordjournals.org/ at University of California, Irvine on April 13, 2016

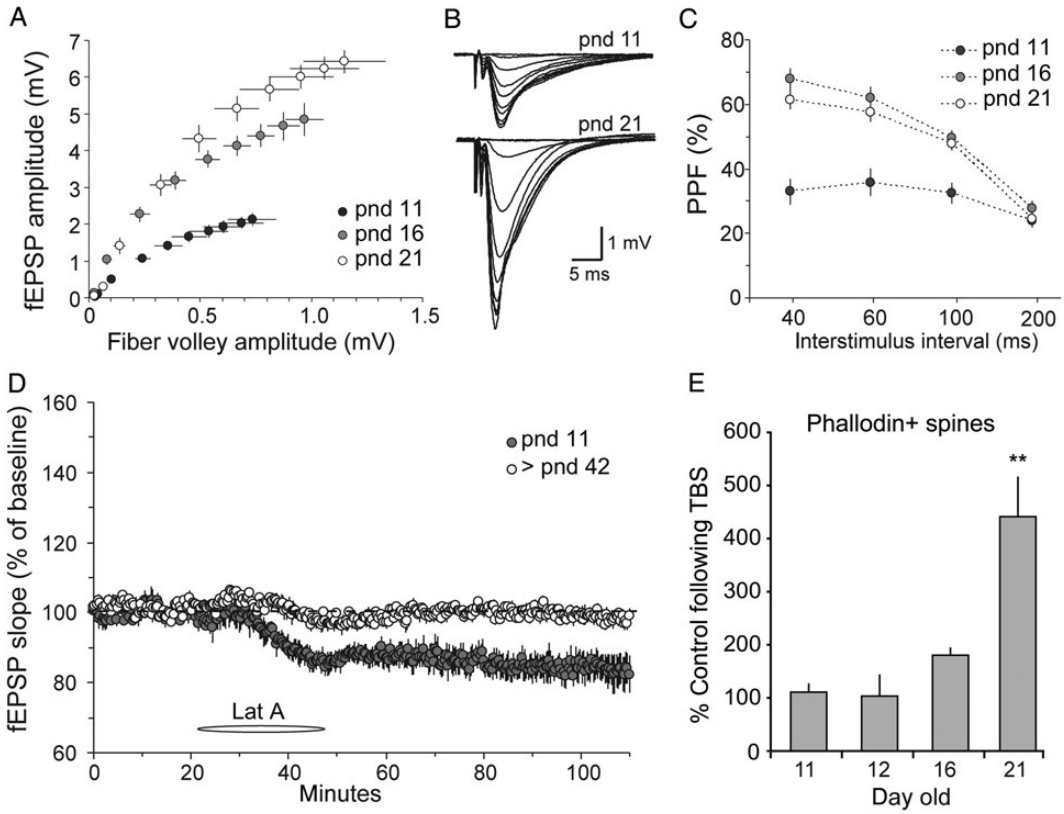

Figure 6. Developmental changes in synaptic physiology and synaptic activity-induced actin polymerization. (*A*) Input/output curves generated in field CA1 compare the amplitudes of the presynaptic fiber volley to the fEPSP across a range of stimulation currents (10–100 μA). Slices from pnd 11 rats show a flatter input/output curve relative to pnd 16 and 21 rats. (*B*) Representative traces of input/output curves recorded in slices from pnd 11 and 21 rat hippocampus. (*C*) Paired-pulse facilitation was smaller in slices from rats at pnd 11 compared with pnd 16 and 21 (plot shows the initial slope of the second synaptic response expressed as percent of the first). (*D*) Infusion of Latrunculin A (Lat A, 200 nM, at horizontal bar) caused significantly greater depression of baseline synaptic transmission in pnd 11 slices relative to those from young adults (>42 days of age: >pnd 42). (*E*) Quantification of phalloidin-labeled spine heads following S–C theta burst stimulation (TBS) in slices from 11- to 21-day-old rats expressed as a percent of values from age-matched slices that received low-frequency control stimulation. Graph shows a dramatic TBS-induced increase in F-actin-enriched spines at pnd 21 only; mean ± SEM values shown ($P = 0.0004$, 1-way ANOVA, $^{**}P < 0.001$ vs. other ages, Tukey multiple comparisons test). The pnd 11–16 groups were not statistically different from each other ($P > 0.05$). Quantification from the CA1 str. radiatum field of electrophysiological recordings.

threonine phosphorylation, as investigated here, is required for activating the Arp2/3 complex to nucleate actin filament branching (LeClaire et al. 2008). Overall, the results strongly suggest that changes in actin management cause the hippocampus to transition between a condition that promotes growth but not stability to one that exhibits less growth but favors stable structures.

The dramatic Week 3 changes seen for cofilin were unusual; none of the other actin-related proteins sampled here underwent such pronounced adjustments. Nonetheless, we were able to identify 4 factors that are likely contributors to the cofilin effect: reductions in protein levels for β1 integrins, pTrkB, and LIMK 2b, and an increase in levels of the phosphatase SSH3. BDNF, acting on TrkB, and integrins both drive spine cofilin phosphorylation in adults in part through the RhoA > RhoA kinase > LIM kinase cascade (Kramar et al. 2009; Rex et al. 2009). SSH (isoforms 1–3) is a major phosphatase that regulates the phosphorylated state of cofilin (Mizuno 2013). We propose that 50% changes in each of these proteins sum to produce the observed, much larger shift in the state of cofilin and so the loss of actin filament formation needed for spine development and synaptogenesis. Whether these changes in brain during Week 3 are secondary consequences of a very large number of effects occurring earlier in development or instead can be linked to a limited set of salient factors is a fascinating question for future research.

Pertinent to the above, it is noteworthy that glia undergo pronounced maturation from the second through third postnatal week (Bushong et al. 2004; Bandeira et al. 2009), and recent work has documented potent interactions between these cells and synapses (Halassa et al. 2009; Pérez-Alvarez and Araque 2013). However, we found that adenosine A1 receptors, which are important mediators of astrocytic actions on synapses (Huang et al. 2001; Rex et al. 2005; Pickel et al. 2006; Wall and Dale 2013) decrease during the period of cofilin dephosphorylation. This is a very surprising result from 2 perspectives: 1) A1Rs decrease at the same time as astrocyte membranes, and so a source for released adenosine (via breakdown of released ATP by the glial ecto-enzyme CD73), are undergoing a massive expansion (Butt and Ransom 1993; Bushong et al. 2004) and 2) A1Rs block synaptic signaling cascades leading to spine cofilin phosphorylation (Rex et al. 2009). The developmental changes in the receptors are therefore not logical contributors to the cofilin effect and indeed would be expected to act against it.

Another factor potentially contributing to the postnatal decline in pCofilin levels is the extracellular matrix protein reelin: not only do expression levels of reelin in brain decrease during the early postnatal period (D'Arcangelo et al. 1995; Schiffmann et al. 1997; Alcántara et al. 1998), but this protein also is involved in the relevant actin signaling pathways (Chai et al. 2009). During

Downloaded from http://cercor.oxfordjournals.org/ at University of California, Irvine on April 13, 2016

early postnatal development, reelin is secreted by Cajal–Retzius cells; in the hippocampus, these cells are located in stratum lacunosum moleculare and what is termed the "outer marginal layer" of the dentate gyrus. As reelin induces phosphorylation of LIMK1 and cofilin (Chai et al. 2009), it is possible that during the early postnatal period reelin contributes to the heightened levels of pCofilin-ir, particularly in the dentate gyrus molecular layer where levels were high at pnd 10 (Fig. 4). By the second postnatal week, Cajal–Retzius cells begin to degenerate (Derer and Derer 1990) and reelin expression falls (D'Arcangelo et al. 1995; Schiffmann et al. 1997; Alcántara et al. 1998). Such a reduction in reelin could contribute to the dramatic decrease in pCofilin during the same period as described here; future studies are needed to evaluate this possibility.

Determinate growth is generally assumed by biologists to reflect strong evolutionary pressures for matching the size of animals to particular ecological niches and life styles. This has evident advantages but, at least for mammals, also has negative consequences. The termination of growth temporally correlates with a loss of reactive growth capacity, as described in studies on axon sprouting and spine reformation after partial deafferentation of hippocampal dendrites (Lynch et al. 1973; Gall and Lynch 1980, 1981). Notably, while the most dramatic changes occur during Week 3 (e.g., the quickness of reactive growth and the length of new collaterals), the rate of synapse replacement continues to slow until Month 3. A number of variables studied here also decrease slightly at least to Day 42. In any event, the end of synapse addition and dendritic extension largely eliminates a capacity that could be useful in ameliorating the effects of brain injury.

Finally, there is the question of whether a precipitous decrease in synaptogenesis has benefits other than niche matching. Rapid encoding of very persistent memory using synapses as storage elements would be difficult in a dynamic population of connections, and consistent with this point, past results supplemented with data reported here demonstrate that stable LTP emerges at the end of Week 3 (Kramar and Lynch 2003). As noted, the phosphorylated (active) Arp2/3 complex increases while phosphorylated cofilin decreases. Theta burst stimulation in young adults quickly phosphorylates synaptic cofilin in association with increases in actin polymerization, but this is followed by a several minute period in which the new filaments and LTP are unstable (Kramar and Lynch 2003; Rex et al. 2005, 2007, 2010; Kramar et al. 2006; Lynch et al. 2007). Phospho-Arp2/3 initiates filament branching and stabilization in many types of cells and so can be assumed to play this role in spines (Rácz and Weinberg 2008). In all, events that suppress growth open the way for rapid and lasting modifications. In this sense, prominent forms of mammalian memory with great survival value could be secondary to other adaptations rather than themselves being a primary target of evolutionary pressures: an "exaptation" in the terminology of Gould and Vrba (1982).

Funding

This work was supported by the National Institute of Neurological Disorders and Stroke (NS045260, NS085709); National Institute of Mental Health (MH101491); the National Science Foundation (fellowships DGE1321846 to C.A.K. and DGE0808392 to C.D.C); and the UCI Center for Autism Research and Translation.

Notes

The authors thank Dr Jihua Liu and Ms Yue Qin Yao for expert technical assistance. *Conflict of Interest*: None declared.

References

Alcántara S, Ruiz M, D'Arcangelo G, Ezan F, de Lecea L, Curran T, Sotelo C, Soriano E. 1998. Regional and cellular patterns of reelin mRNA expression in the forebrain of the developing and adult mouse. J Neurosci. 18:7779–7799.

Ammer AG, Weed SA. 2008. Cortactin branches out: roles in regulating protrusive actin dynamics. Cell Motil Cytoskeleton. 65:687–707.

Aoki C, Miko I, Oviedo H, Mikeladze-Dvali T, Alexandre L, Sweeney N, Bredt DS. 2001. Electron microscopic immunocytochemical detection of PSD-95, PSD-93, SAP-102, and SAP-97 at postsynaptic, presynaptic, and nonsynaptic sites of adult and neonatal rat visual cortex. Synapse. 40:239–257.

Arikkath J. 2012. Molecular mechanisms of dendrite morphogenesis. Front Cell Neurosci. 6:61.

Bamburg JR. 1999. Proteins of the ADF/cofilin family: essential regulators of actin dynamics. Annu Rev Cell Dev Biol. 15:185–230.

Bandeira F, Lent R, Herculano-Houzel S. 2009. Changing numbers of neuronal and non-neuronal cells underlie postnatal brain growth in the rat. Proc Natl Acad Sci USA. 106:14108–14113.

Bernstein B, Bamburg J. 2010. ADF/cofilin: a functional node in cell biology. Trends Cell Biol. 20:187–195.

Bramham CR. 2008. Local protein synthesis, actin dynamics, and LTP consolidation. Curr Opin Neurobiol. 18:524–531.

Bushong EA, Martone ME, Ellisman MH. 2004. Maturation of astrocyte morphology and the establishment of astrocyte domains during postnatal hippocampal development. Int J Dev Neurosci. 22:73–86.

Butt AM, Ransom BR. 1993. Morphology of astrocytes and oligodendrocytes during development in the intact rat optic nerve. J Comp Neurol. 338:141–158.

Chai X, Förster E, Zhao S, Bock H, Frotscher M. 2009. Reelin stabilizes the actin cytoskeleton of neuronal processes by inducing n-cofilin phosphorylation at serine3. J Neurosci. 29:288–299.

Chan AY, Bailly M, Zebda N, Segall JE, Condeelis JS. 2000. Role of cofilin in epidermal growth factor-stimulated actin polymerization and lamellipod protrusion. J Cell Biol. 148:531–542.

Chen L, Rex C, Babayan A, Kramár E, Lynch G, Gall C, Lauterborn J. 2010. Physiological activation of synaptic Rac>PAK (p-21 activated kinase) signaling is defective in a mouse model of fragile X syndrome. J Neurosci. 30:10977–10984.

Chen LY, Rex CS, Casale MS, Gall CM, Lynch G. 2007. Changes in synaptic morphology accompany actin signaling during LTP. J Neurosci. 27:5363–5372.

Cooper JA. 1987. Effects of cytochalasin and phalloidin on actin. J Cell Biol. 105:1473–1478.

Courtemanche N, Gifford SM, Simpson MA, Pollard TD, Koleske AJ. 2015. Abl2/Abl-related gene stabilizes actin filaments, stimulates actin branching by actin-related protein 2/3 complex, and promotes actin filament severing by cofilin. J Biol Chem. 290:4038–4046.

Cowan WM, Stanfield BB, Kishi K. 1980. The development of the dentate gyrus. In: Hunt KR, editor. Neural development, part I. San Francisco: Academic Press. p. 103–157.

Crain B, Cotman C, Taylor D, Lynch G. 1973. A quantitative electron microscopic study of synaptogenesis in the dentate gyrus of the rat. Brain Res. 63:195–204.

D'Arcangelo G, Miao G, Chen S, Soares H, Morgan J, Curran T. 1995. A protein related to extracellular matrix proteins deleted in the mouse mutant reeler. Nature. 374:719–723.

Derer P, Derer M. 1990. Cajal-Retzius cell ontogenesis and death in mouse brain visualized with horseradish peroxidase and electron microscopy. Neuroscience. 36:839–856.

Downloaded from http://cercor.oxfordjournals.org/ at University of California, Irvine on April 13, 2016

Dudek SM, Johnson GVW. 1995. Postnatal changes in serine/threnonine protein phosphatases and their association with the microtubules. Dev Brain Res. 90:54–61.
Fischer M, Kaech S, Knutti D, Matus A. 1998. Rapid actin-based plasticity in dendritic spines. Neuron. 20:847–854.
Gall C, Lynch G. 1981. Fiber architecture of the dentate gyrus following ablation of the entorhinal cortex in rats of different ages: evidence for two forms of axon sprouting in the immature brain. Neuroscience. 6:903–910.
Gall CM, Lynch G. 1980. The regulation of fiber growth and synaptogenesis in the developing hippocampus. Curr Top Dev Biol. 15:159–180.
Gohla A, Birkenfeld J, Bokoch GM. 2005. Chronophin, a novel HAD-type serine protein phosphatase, regulates cofilin-dependent actin dynamics. Nat Cell Biol. 7:21–29.
Gould SJ, Vrba ES. 1982. Exaptation; a missing term in the science of form. Paleobiology. 8:4–15.
Halassa MM, Fellin T, Haydon PG. 2009. Tripartite synapses: roles for astrocytic purines in the control of synaptic physiology and behavior. Neuropharmacology. 57:343–346.
Harris K, Teyler T. 1984. Developmental onset of long-term potentiation in area CA1 of the rat hippocampus. J Physiol. 346:27–48.
Hotulainen P, Hoogenraad CC. 2010. Actin in dendritic spines: connecting dynamics to function. J Cell Biol. 189:619–629.
Huang CC, Liang YC, Hsu KS. 2001. Characterization of the mechanism underlying the reversal of long term potentiation by low frequency stimulation at hippocampal CA1 synapses. J Biol Chem. 276:48108–48117.
Hunt CA, Schenker LJ, Kennedy MB. 1996. PSD-95 is associated with the postsynaptic density and not with the presynaptic membrane at forebrain synapses. J Neurosci. 16:1380–1388.
Isomura Y, Kato N. 1999. Action potential-induced dendritic calcium dynamics correlated with synaptic plasticity in developing hippocampal pyramidal cells. J Neurophysiol. 82:1993–1999.
Jackson PS, Suppes T, Harris KM. 1993. Stereotypical changes in the pattern and duration of long-term potentiation expressed at postnatal days 11 and 15 in the rat hippocampus. J Neurophysiol. 70:1412–1419.
Jan YN, Jan LY. 2010. Branching out: mechanisms of dendritic arborization. Nat Rev Neurosci. 11:316–328.
Kedrin D, van Rheenen J, Hernandez L, Condeelis J, Segall JE. 2007. Cell motility and cytoskeletal regulation in invasion and metastasis. J Mammary Gland Biol Neoplasia. 12:143–152.
Kennedy MB. 1997. The postsynaptic density at glutamatergic synapses. Trends Neurosci. 20:264–268.
Komagome R, Kimura K, Saito M. 2000. Postnatal changes in Rho and Rho-related proteins in the mouse brain. Jpn J Vet Res. 47:127–133.
Koskinen M, Bertling E, Hotulainen R, Tanhuanpää K, Hotulainen P. 2014. Myosin IIb controls actin dynamics underlying the dendritic spine maturation. Mol Cell Neurosci. 61:56–64.
Kramar EA, Chen LY, Brandon NJ, Rex CS, Liu F, Gall CM, Lynch G. 2009. Cytoskeletal changes underlie estrogen's acute effects on synaptic transmission and plasticity. J Neurosci. 29:12982–12993.
Kramar EA, Lin B, Rex CS, Gall CM, Lynch G. 2006. Integrin-driven actin polymerization consolidates long-term potentiation. Proc Natl Acad Sci USA. 103:5579–5584.
Kramar EA, Lynch G. 2003. Developmental and regional differences in the consolidation of long-term potentiation. Neuroscience. 118:387–398.
Lafont F, Rouget M, Rousselet A, Valenza C, Prochiantz A. 1993. Specific responses of axons and dendrites to cytoskeleton perturbations: an in vitro study. J Cell Sci. 104(Pt 2):433–443.
Lanoue V, Usardi A, Sigoillot SM, Talleur M, Iyer K, Mariani J, Isope P, Vodjdani G, Heintz N, Selimi F. 2013. The adhesion-GPCR BAI3, a gene linked to psychiatric disorders, regulates dendrite morphogenesis in neurons. Mol Psychiatry. 18:943–950.
Laver RJ, Purwandana D, Ariefiandy A, Imansyah J, Forsyth D, Ciofi C, Jessop TS. 2012. Life-history and spatial determinants of somatic growth dynamics in Komodo dragon populations. PLoS One. 7:e45398.
LeClaire LL 3rd, Baumgartner M, Iwasa JH, Mullins RD, Barber DL. 2008. Phosphorylation of the Arp2/3 complex is necessary to nucleate actin filaments. J Cell Biol. 182:647–654.
Liao D, Malinow R. 1996. Deficiency in induction but not expression of LTP in hippocampal slices from young rats. Learn Mem. 3:138–149.
Lin B, Kramar EA, Bi X, Brucher FA, Gall CM, Lynch G. 2005. Theta stimulation polymerizes actin in dendritic spines of hippocampus. J Neurosci. 25:2062–2069.
Lynch G, Rex CS, Gall CM. 2007. LTP consolidation: substrates, explanatory power, and functional significance. Neuropharmacology. 52:12–23.
Lynch GS, Stanfield B, Cotman CW. 1973. Developmental differences in postlesion axonal growth in the hippocampus. Brain Res. 59:155–168.
Mizuno K. 2013. Signaling mechanisms and functional roles of cofilin phosphorylation and dephosphorylation. Cell Signal. 25:457–469.
Moriyama K, Iida K, Yahara I. 1996. Phosphorylation of Ser-3 of cofilin regulates its essential function on actin. Genes Cells. 1:73–86.
Muller D, Oliver M, Lynch G. 1989. Developmental changes in synaptic properties in hippocampus of neonatal rats. Brain Res Dev Brain Res. 49:105–114.
Niwa R, Nagata-Ohashi K, Takeichi M, Mizuno K, Uemura T. 2002. Control of actin reorganization by Slingshot, a family of phosphatases that dephosphorylate ADF/cofilin. Cell. 108:233–246.
Okamoto K, Narayanan R, Lee SH, Murata K, Hayashi Y. 2007. The role of CaMKII as an F-actin-bundling protein crucial for maintenance of dendritic spine structure. Proc Natl Acad Sci USA. 104:6418–6423.
O'Kusky JR, Ye P, D'Ercole AJ. 2000. Insulin-like growth factor-I promotes neurogenesis and synaptogenesis in the hippocampal dentate gyrus during postnatal development. J Neurosci. 20:8435–8442.
Pak CW, Flynn KC, Bamburg JR. 2008. Actin-binding proteins take the reins in growth cones. Nat Rev Neurosci. 9:136–147.
Patnaik BK. 1994. Ageing in reptiles. Gerontology. 40:200–220.
Pérez-Alvarez A, Araque A. 2013. Astrocyte-neuron interaction at tripartite synapses. Curr Drug Targets. 14:1220–1224.
Petralia RS, Sans N, Wang YX, Wenthold RJ. 2005. Ontogeny of postsynaptic density proteins at glutamatergic synapses. Mol Cell Neurosci. 29:436–452.
Pickel VM, Chan J, Linden J, Rosin DL. 2006. Subcellular distributions of adenosine A1 and A2A receptors in the rat dorsomedial nucleus of the solitary tract at the level of the area postrema. Synapse. 60:496–509.
Rácz B, Weinberg RJ. 2008. Organization of the Arp2/3 complex in hippocampal spines. J Neurosci. 28:5654–5659.
Racz B, Weinberg RJ. 2006. Spatial organization of cofilin in dendritic spines. Neuroscience. 138:447–456.

Downloaded from http://cercor.oxfordjournals.org/ at University of California, Irvine on April 13, 2016

Rex CS, Chen LY, Sharma A, Liu J, Babayan AH, Gall CM, Lynch G. 2009. Different Rho GTPase-dependent signaling pathways initiate sequential steps in the consolidation of long-term potentiation. J Cell Biol. 186:85–97.

Rex CS, Gavin CF, Rubio MD, Kramar EA, Chen LY, Jia Y, Huganir RL, Muzyczka N, Gall CM, Miller CA, et al. 2010. Myosin IIb regulates actin dynamics during synaptic plasticity and memory formation. Neuron. 67:603–617.

Rex CS, Kramar EA, Colgin LL, Lin B, Gall CM, Lynch G. 2005. Long-term potentiation is impaired in middle-aged rats: regional specificity and reversal by adenosine receptor antagonists. J Neurosci. 25:5956–5966.

Rex CS, Lin CY, Kramar EA, Chen LY, Gall CM, Lynch G. 2007. Brain-derived neurotrophic factor promotes long-term potentiation-related cytoskeletal changes in adult hippocampus. J Neurosci. 27:3017–3029.

Rudy JW. 2015. Actin dynamics and the evolution of the memory trace. Brain Res. 1621:17–28.

Schiffmann S, Bernier B, Goffinet A. 1997. Reelin mRNA expression during mouse brain development. Eur J Neurosci. 9:1055–1071.

Seese R, Chen L, Cox C, Schulz D, Babayan A, Bunney W, Henn F, Gall C, Lynch G. 2013. Synaptic abnormalities in the infralimbic cortex of a model of congenital depression. J Neurosci. 33:13441–13448.

Seese RR, Babayan AH, Katz AM, Cox CD, Lauterborn JC, Lynch G, Gall CM. 2012. LTP induction translocates cortactin at distant synapses in wild-type but not Fmr1 knock-out mice. J Neurosci. 32:7403–7413.

Sun CX, Magalhaes MA, Glogauer M. 2007. Rac1 and Rac2 differentially regulate actin free barbed end formation downstream of the fMLP receptor. J Cell Biol. 179:239–245.

Trieu BH, Kramar EA, Cox CD, Jia Y, Wang W, Gall CM, Lynch G. 2015. Pronounced differences in signal processing and synaptic plasticity between piriform-hippocampal network stages: a prominent role for adenosine. J Physiol. 593: 2889–2907.

van Rheenen J, Condeelis J, Glogauer M. 2009. A common cofilin activity cycle in invasive tumor cells and inflammatory cells. J Cell Sci. 122:305–311.

van Rheenen J, Song X, van Roosmalen W, Cammer M, Chen X, Desmarais V, Yip SC, Backer JM, Eddy RJ, Condeelis JS. 2007. EGF-induced PIP2 hydrolysis releases and activates cofilin locally in carcinoma cells. J Cell Biol. 179:1247–1259.

Wall MJ, Dale N. 2013. Neuronal transporter and astrocytic ATP exocytosis underlie activity-dependent adenosine release in the hippocampus. J Physiol. 591:3853–3871.

Wang W, Eddy R, Condeelis J. 2007. The cofilin pathway in breast cancer invasion and metastasis. Nat Rev Cancer. 7:429–440.

Wang XB, Bozdagi O, Nikitczuk JS, Zhai ZW, Zhou Q, Huntley GW. 2008. Extracellular proteolysis by matrix metalloproteinase-9 drives dendritic spine enlargement and long-term potentiation coordinately. Proc Natl Acad Sci USA. 105:19520–19525.

Wasling P, Hanse E, Gustafsson B. 2004. Developmental changes in release properties of the CA3-CA1 glutamate synapse in rat hippocampus. J Neurophysiol. 92:2714–2724.

Yarmola EG, Somasundaram T, Boring TA, Spector I, Bubb MR. 2000. Actin-Latrunculin A structure and function. J Biol Chem. 275:28120–28127.

Zhong JL, Banerjee MD, Nikolic M. 2003. Pak1 and its T212 phosphorylated form accumulate in neurones and epithelial cells of the developing rodent. Dev Dyn. 228:121–127.

Zimmer J, Haug FM. 1978. Laminar differentiation of the hippocampus, fascia dentata and subiculum in developing rats, observed with the Timm sulphide silver method. J Comp Neurol. 179:581–617.

Zucker R, Regehr W. 2002. Short-term synaptic plasticity. Annu Rev Physiol. 64:355–405.

Downloaded from http://cercor.oxfordjournals.org/ at University of California, Irvine on April 13, 2016